Study of MgO transformation into MgF₂ in the presence of CF₂Cl₂•

ALEKSEY A. VEDYAGIN[1,2]*, ALEXANDER F. BEDILO[1,3], ILYA V. MISHAKOV[1,2]
and EKATERINA I. SHUVARAKOVA[1,3]

[1]Boreskov Institute of Catalysis, Siberian Branch, Russian Academy of Sciences, Novosibirsk, Russia, [2]National Research Tomsk Polytechnic University, Tomsk, Russia and [3]Novosibirsk Institute of Technology, Moscow State University of Design and Technology, Novosibirsk, Russia

Abstract: Alkaline-earth metal oxide aerogels prepared by sol–gel method followed by autoclave drying are nanocrystalline mesoporous materials with high reactivity. Bulk solid-state reaction of MgO aerogels with CF_2Cl_2 takes place after a long induction period, during which the active sites are accumulated on the surface of the nanoparticles. It was found that vanadium addition has a promoting effect on this reaction accelerating the process of the active sites formation. A method for characterization of electron-acceptor sites by electron spin resonance spectroscopy using perylene as the spin probe was developed. A good correlation was observed between the rate of the CF_2Cl_2 destructive sorption and the concentration of weak electron-acceptor sites. Simplified models of such sites were suggested. The acid sites on the modified MgO surface were supposed to be originated from separation of the charged fragments resulting in the surface polarization. Uncompensated oxygen substitution for chlorine and/or fluorine ions leads to appearance of Lewis acid sites while HCl/HF chemisorption results in Bronsted acid sites formation.

Keywords: aerogels; destructive sorption; freon-12; acid sites; spin probe; vanadium.

INTRODUCTION

Halocarbons are very stable compounds which are known to contribute to the ozone layer destruction. Thereby, development of active materials for their decomposition without harming the environment is of substantial practical imp-

---

ortance. From this point of view, alkaline-earth metal oxide aerogels are particularly interesting nanocrystalline mesoporous materials, effective in decomposition of toxic substances such as organophosphorus compounds and chlorocarbons and show high activity in a number of catalytic reactions.[1–10]

Klabunde *et al.* earlier studied the effect of different transition metal promoters on the CCl_4 decomposition over aerogel-prepared MgO (AP-MgO) and showed that the promoter effectiveness increased in the following order: Sc < < none < Cr < Ni < Cu < Ti < Zn < Fe < Co < Mn < V.[11] The catalytic effects were proposed to be due to the intermediacy of transition metal chlorides. V_2O_5/MgO sample demonstrated the highest activity, which was later also observed for the reactions with $CFCl_3$ and CF_2Cl_2.[12–14]

Superior adsorption properties of nanocrystalline MgO aerogels are often attributed to high concentration of low-coordinated surface sites.[1] However, it is known that the surface of partially hydroxylated MgO contains various surface active sites with different properties.[15–21] So, the origin of the sites active in different processes initiated on its surface should be studied in detail.

Electron-donor and electron-acceptor sites studied by electron paramagnetic resonance (EPR) using suitable spin probes are well known in the literature.[22–26] Aromatic nitro compounds are frequently used as the probe molecules for investigation of the electron-donor sites on such oxide supports as Al_2O_3, MgO, ZrO_2, etc. due to their pronounced electron-acceptor properties and formation of stable radical anions.[16,19,25,27,28] Electron-acceptor sites are the sites capable of generating radical cations from aromatic donor molecules by abstracting a single electron from them.[22] The formed radical cations can either be observed by EPR directly or can participate in reactions leading to the formation of secondary paramagnetic products on the surface.[22,26,29–34] The strength of the surface acceptor sites can be qualitatively characterized by selecting probe molecules with different ionization potentials.[26]

In the current paper, we summarize our previously published and new results on the reactivity of aerogel MgO (AP-MgO) with CF_2Cl_2. The vanadium effect on the reactivity of mesoporous MgO aerogels and duration of the induction period (IP) in the reaction with difluorodichloromethane is analyzed. The reaction kinetics and products obtained over MgO and VO_x·MgO aerogels with different vanadium concentrations are compared. The obtained data prove that the active reaction stage is initiated on some active sites. Changes in the concentrations of surface electron-donor and electron-acceptor sites during the reaction of the MgO aerogel with CF_2Cl_2 are studied. Electron-acceptor sites were characterized by electron spin resonance spectroscopy using perylene as the spin probe for a first time. The obtained results suggest that weak electron-acceptor sites formed during the induction period may account for the active stage of the process.

EXPERIMENTAL

Magnesium methoxide was prepared by dissolving Mg metal ribbon (Fisher) in methanol. Usually 1 M solution was prepared by the reaction of 4.86 g (0.20 mol) Mg with 206 ml methanol at room temperature under nitrogen flow. For preparation of modified MgO aerogels, magnesium methoxide solution obtained at the first step was diluted with a desired amount of methanol and/or another solvent (*e.g.*, toluene). Then, the solution of the modifying agent in 10 ml methanol was quickly poured into the reaction vessel with magnesium methoxide and the resulting mixture was stirred for 10 min. Finally, a stoichiometric amount of hydrolysis water dissolved in methanol was added dropwise and a gel was formed. The reaction vessel was continuously maintained under nitrogen flow during the whole reaction.

The aerogels were prepared by high temperature supercritical drying of the gels in a standard one-liter autoclave (Parr). The autoclave temperature was increased to a desired value at the rate of 1 °C per minute and maintained at that temperature for 10 min. The final pressure was about 7000 kPa. Then, the pressure was quickly released by venting of solvent vapor.

For preparation of mixed V–MgO aerogels, vanadium (V) triisopropoxide oxide was added to the fresh $Mg(OH)_2$ gel and stirred. Then, the obtained mixed gel was dried in an autoclave to remove the solvents under supercritical conditions. The synthesized V–$Mg(OH)_x$ aerogels were calcined on air in a temperature-programmed regime. This procedure yielded mesoporous $VO_x·MgO$ materials with high surface area (~ 400 m^2/g) and average pore size 8–12 nm. Samples with vanadium loading in a range of 1–10 wt. % (normalized to V_2O_5) were synthesized.

Reference V_2O_5/AP-MgO samples were prepared by grinding AP-MgO with ammonium vanadate (Aldrich) in a ceramic mortar. Then, the samples were heated under vacuum at 450––600 °C for 2 h with gradual temperature increase. During the heating ammonium vanadate melted filling the AP-MgO pores and then decomposed to vanadium (V) oxide. After calcination the sample was slowly cooled down to room temperature under continuous evacuation.

Decomposition of the halocarbons over prepared samples was studied in a temperature range of 300–450 °C. In the most experiments, a flow reactor with a McBain spring balance equipped with an on-line gas chromatograph was used. This installation made it possible to monitor continuously the sample weight and occasionally study the gas-phase composition. Pure-grade CF_2Cl_2 and $CFCl_3$ and high purity argon were used in the experiments. The Ar purity was no less than 99.99 % with oxygen concentration less than 0.001 % and water content below 0.1 g/m^3. A sample (100 mg) was placed into the basket of the spring balance. Prior to the reaction the sample was activated at 500°C for 30 min. The halocarbons were passed through the reactor with a rate of 3 l/h.

Some experiments on study of CF_2Cl_2 interaction with nanocrystalline oxides were provided using a TEOM (tapered element oscillating microbalance) 1500 PMA gravimetric microanalyzer. The TEOM microanalyzer uses a unique principle for measuring mass based on the relationship between the oscillation frequency of a pendulum-microreactor and the weight of the studied sample.[26] The precision of the weight measurement is $5×10^{-6}$ g with the maximum measurement frequency 0.1 Hz.

High purity helium (99.9999 %) and CF_2Cl_2 with 98 % purity were used in the TEOM experiments. Before an experiment the sample was heated in the helium flow at 500 °C until a constant mass was obtained. Then, the sample was cooled down to the reaction temperature. Thereafter, the flow gas was changed for CF_2Cl_2. Composition of the outlet gases was analyzed using a quadrupole mass-spectrometer QMS-200.

Specific surface areas and average pore volumes before and after reaction were determined by low-temperature adsorption of argon using an ASAP-2400 instrument. The XRD analysis of the samples was carried out using an X'TRA (Thermo ARL) instrument in the air in the 2θ range of 5–80° with 0.05° step and 5 s accumulation time at each point. The crystallite sizes D_{hkl} were calculated by the Scherer method.

Transmission electron microscopy (TEM) images were obtained using a JEOL JEM--2010 electron microscope with lattice resolution 0.14 nm at accelerating voltage 200 kV. The local energy-dispersion X-ray (EDX) microanalysis was carried out using EDAX spectrometer with energy resolution 127 eV.

The EPR experiments were conducted using the EPR installation described in detail elsewhere.[32] An ERS-221 spectrometer was used for registration of the X-band ESR spectra at room temperature. The concentrations of the paramagnetic species were determined by numerical double integration with baseline compensation. DPPH and Cu^{2+} standards were used for calibration.

The concentration of electron-donor and electron-acceptor sites during the CF_2Cl_2 destructive sorption were measured using the following original procedure. A sample was loaded in an EPR tube, which was placed into a catalytic installation equipped with a furnace and gas flow controllers. A thin metal capillary used for gases feeding to the sample was placed inside the EPR tube. Prior to the reaction the sample was heated in 30 ml/min nitrogen flow to the reaction temperature. Then, the gas flow was switched for CF_2Cl_2. After desired time, the gas flow was switched back to nitrogen, and the sample was purged with nitrogen for 2 min. Then, the EPR tube with the sample after reaction was taken out from the installation, quickly cooled to room temperature and filled with a toluene solution of the selected spin probe.

1,3,5-Trinitrobenzene (TNB), anthracene and perylene were used for characterization of electron-donor site and electron-acceptor sites, respectively. The spin probes were adsorbed from 2 x 10^{-2} M solutions in toluene. The first EPR spectrum was recorded immediately after the spin probe was adsorbed. Then, the samples with the solution of the spin probe were heated at 80 °C for 18–20 h before registering another EPR spectrum. All the EPR spectra were recorded at room temperature.

RESULTS AND DISCUSSION

Modification of Mg(OH)₂ and MgO aerogels

Organic groups can be used for modification of typical metal alkoxide precursors in the sol–gel process to alter reaction rates of reactants, control homogeneity and microstructure of the formed gels or functionalize the oxide material. We studied the effect of several acids, and β-diketones as well as toluene in the magnesium methoxide solution on the gelation and properties of the MgO aerogels. Strong complexing agents, such as β-diketones, polyhydroxylated ligands and hydroxyacids have been successfully used for synthesis of modified zirconia and titania gels.[35,36] After hydrolysis many of such groups remain bound to metal atoms while alkoxy groups are quickly removed.

Similar to zirconia and titania gels, addition of acetylacetone, acetic acid and HNO_3 prevented precipitation and resulted in a noticeable increase of the gel time and often the formation of nice clear gels. Hard clear gels, which are often desirable during the synthesis of other metal oxide aerogels, could be easily

obtained at $Mg(OCH_3)_2$ concentration of 0.5 M after the acid addition.[37–39] Unfortunately, modification of $Mg(OH)_2$ aerogels with such modifiers as acetic acid, benzoic acid, nitric acid, acetylacetone or benzoylacetone yielded materials with low surface areas in the range of 50–100 m^2/g.

Toluene presence was claimed to accelerate both the hydrolysis and gelation reactions.[40] The use of toluene and other aromatic compounds such as benzene and mesitylene as co-solvents resulted in the formation of clear gels eliminating the need for addition of acids and a considerable increase in the surface area of resulting $Mg(OH)_2$ aerogels up to 1150 m^2/g.[41]

Although toluene is not the only aromatic compound with such effect, it is the most convenient for practical use as it is less toxic than benzene and more volatile than heavier organic solvents. The autoclave temperature of 265 °C used in the standard procedure for the preparation of AP–MgO is above critical for methanol, but not for toluene. Although the surface tension of toluene is not completely eliminated under these conditions, it does not have a significant negative effect on the aerogel properties.

Dehydration of $Mg(OH)_2$ aerogels is usually performed by heating under vacuum at 500 °C.[1,42,43] This procedure yields nanocrystalline AP-MgO samples with the particle sizes of 1-5 nm and surface areas of 400–700 m^2/g. Figure 1 presents TEM images of the AP–MgO sample. At high magnification one can see that the sample consists of 40–60 Å crystallites arranged into chains forming a very porous secondary structure.
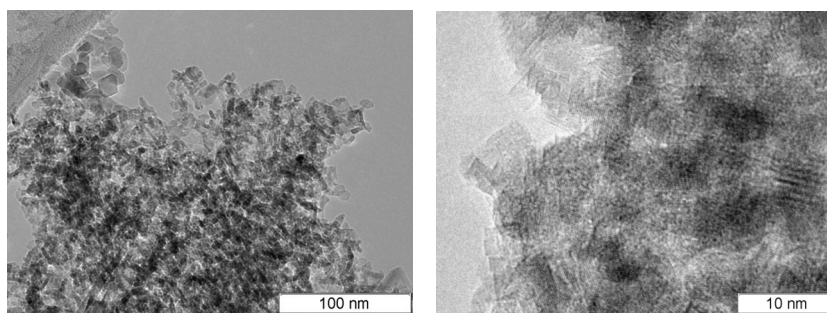

Fig. 1. TEM images with different magnification of AP–MgO sample.

Reaction of Nanocrystalline MgO with CF_2Cl_2

CF_2Cl_2 was found to react with nanoscale MgO starting from 325 °C leading to a significant increase of the sample mass.[3] Typical weight gain kinetic curves are presented in Fig. 2. The most interesting feature of these kinetic curves is the presence of an induction period before the fast weight increase. Note that the IP phenomenon was reproducible with ca. 10 % accuracy. According to the data shown in Figs. 2 and 3, both the duration of the induction period and degree of

MgO conversion were found to be a function on the reaction temperature. It is seen that intensity of the reflexes in XRD patterns (Fig. 3) corresponded to MgO phase (JCPDS card No. 87-0653) diminishes along with reaction temperature rise.
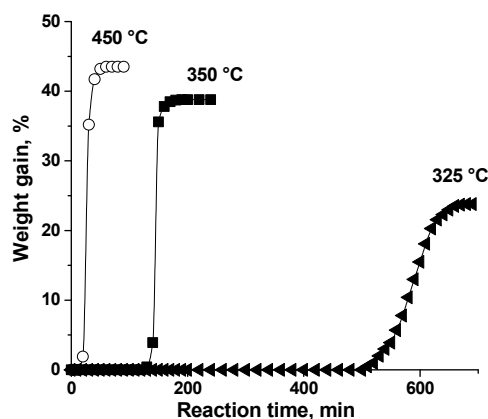

Fig. 2. Kinetic curves of the AP–MgO weight gain during reaction with CF_2Cl_2 at different temperatures.
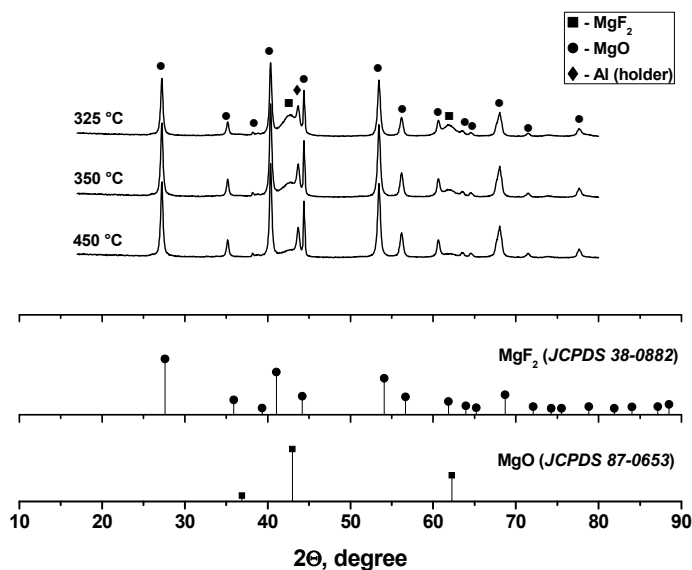

Fig. 3. XRD patterns for AP–MgO sample after reaction with CF_2Cl_2 at 325, 350 and 450 °C, and reference patterns for MgO (JCPDS card No. 87-0653) and MgF_2 (JCPDS card No. 38-0882).

The IP phenomenon was recently reported to be related to gradual formation of some active sites or defects on the MgO surface. Intense bulk substitution of oxygen by fluorine starts only when such active sites are accumulated in sufficiently high concentration. According to the EDX results, both chlorine and

fluorine are incorporated into MgO in comparable amounts during the IP.[3] The TEM and EDX data show that the crystalline $MgCl_2$ is not formed. It was proposed there that chlorine exists in the form of adsorbed species and defective oxyhalide structures with variable amounts of halogen atoms partially substituting oxygen atoms of MgO.

According to the XRD studies, the samples after reaction consisted of MgF_2 and some unreacted MgO. TEM showed the presence of particles with two very different morphologies.[3] Large irregular particles with the size from 100 to 300 nm and clusters of small relatively uniform particles with the size about 50 nm were present. The EDX data showed that the clusters consisted mostly of MgO that is only partially converted to MgF_2. Meanwhile, the larger particles consisted of almost pure MgF_2 with very low concentration of oxygen.[3]

In all cases the surface areas of the samples after reaction are significantly lower than that of the initial AP-MgO (380 m^2/g). This is due to intense sintering of both the initial magnesium oxide and resulting magnesium fluoride. The surface area of the sample with the weight gain of only 2.5 % after reaction at 350 °C is already as low as 77 m^2/g, going down to 15 m^2/g after the reaction was complete.

The reaction of AP–MgO with CF_2Cl_2 in a closed container was studied by GC–MS. During the induction period the CF_2Cl_2 conversion was low. The main products were CO_2 and $CFCl_3$ formed in ca. 1:1 ratio. The ratio between the products at this stage indicates that chlorination of the MgO surface takes place during the induction period in addition to the magnesium fluoride formation on the surface. Two independent reactions (1) and (2) seem to take place.

$$2MgO + CF_2Cl_2 \rightarrow MgF_2 + MgCl_2 + CO_2 \qquad (1)$$

$$2CF_2Cl_2 + MgCl_2 \rightarrow 2CFCl_3 + MgF_2 \qquad (2)$$
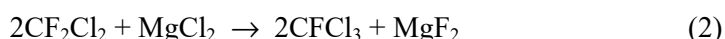
As the concentration of absorbed chloride grows, the $CFCl_3$ and CCl_4 concentrations in the products increase. Chlorine atoms can be exchanged for fluorine in an exothermal process. At some point, the reaction switches to autocatalytic mode when released energy accelerates further MgO fluorination, which is also exothermal.

After completion of the induction period, the CF_2Cl_2 conversion rate substantially increased. Now the main products were CO_2 and CCl_4 formed in 1:1 ratio. This product ratio indicates that $MgCl_2$ formed in reaction (1) is converted to MgF_2 in reaction (3) leading to overall reaction (4).

$$CF_2Cl_2 + MgCl_2 \rightarrow CCl_4 + MgF_2 \qquad (3)$$

$$2MgO + 2CF_2Cl_2 \rightarrow 2MgF_2 + CO_2 + CCl_4 \qquad (4)$$
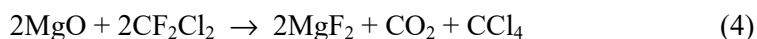
So, an MgO excess is required to convert all CF_2Cl_2 to CO_2 and solid products according to reaction (1). We managed to achieve complete CF_2Cl_2 mineralization at MgO/CF_2Cl_2 ratio 2.5:1.

These observations suggest that some active sites, where the rate of the solid-state reaction is substantially higher than on the other surface sites, must be formed during the induction period. Their high activity must counteract the surface area loss during the induction period. A similar situation was observed by us for catalytic dehydrochlorination of halogenated butanes over AP–MgO.[8,9] In that case surface acid sites formed by the MgO halogenation were by 1–2 orders of magnitude more active than the sites originally present on the MgO surface. As the MgO surface is subjected to halogenation in both cases, the nature of the active sites may be the same.

Synthesis of V-Mg(OH)$_x$ and VO$_x$/MgO aerogels

The synthesis of mixed oxide aerogels by hydrolysis of either mixed alkoxides or a homogeneous solution of two or more individual metal alkoxides followed by supercritical drying is known to yield homogeneous materials with high surface areas and small crystallite sizes.[44,45] We found toluene to be a good second solvent for stabilization of the mixed 10 % V-Mg(OH)$_x$ gel. As follows from Table I, typical surface areas of the mixed aerogels obtained after supercritical drying was about 1100 m^2/g.

TABLE I. Specific surface area (SSA) of the prepared aerogel samples

Sample	Treatment	Temperature, °C	SSA, m^2/g
Mg(OH)$_2$	Autoclave drying	260	1060
2 % V–Mg(OH)$_X$	Autoclave drying	260	1100
10 % V–Mg(OH)$_X$	Autoclave drying	260	1150
10 % VO$_X$–MgO	Calcination (Air, 5 °C/min)	400	525
10 % VO$_X$–MgO	Calcination (Air, 5 °C/min)	500	400
10 % VO$_X$–MgO	Calcination (Air, 5 °C/min)	550	325
2 % VO$_X$–MgO	Calcination (Air, 5 °C/min)	550	300
10 % VO$_X$–MgO	Calcination (Vacuum, 5 °C/min)	550	220
10 % VO$_X$–MgO	Calcination (Ar, 5 °C/min)	550	285
10 % VO$_X$–MgO	Calcination (Ar, 0.5 °C/min)	550	385
10 % VO$_X$–MgO	Calcination (Air, 0.5 °C/min)	550	450

As our aim was to prepare nanocrystalline mixed VO$_x$/MgO oxide with high surface area for use as a catalyst or destructive sorbent at elevated temperatures, we studied the effect of dehydration conditions on the properties of aerogels. However, dehydration of AP-V-Mg(OH)$_x$ samples under vacuum led to the formation of mixed oxides with the surface area below 300 m^2/g (Table I).

By far the simplest dehydration method is the calcination in air. The surface area of the 10 % VO$_x$/MgO sample obtained after calcination at 500 °C was about

400 m^2/g. The surface areas of the mixed oxides prepared by calcination of our hydroxide aerogels exceeded the literature data on the VO$_x$/MgO materials prepared by impregnation even when AP-MgO with high surface area was used as the support.[5,46]

Even higher surface area about 450 m^2/g was obtained when heating was carried out in the air flow using a low heating rate (0.5 °C/min) in the temperature range from 280 to 380 °C. Other experiments showed that the heating rate in the other temperature regions below 280 °C and above 380 °C had a minor effect on the final surface area of the material. So, fast heating with 5 °C/min heating rate could be effectively used in these temperature regions.

Effect of vanadium on the MgO activity in CF$_2$Cl$_2$ destruction

Gravimetric experiments using TEOM showed that addition of just 1% vanadium led to a substantial increase of the MgO reactivity in the reaction with CF$_2$Cl$_2$ (Table II). After the induction period, the rapid reaction was also much faster in the presence of vanadium (12 %/min for MgO and 41 %/min for 1 % VO$_x$·MgO). The acceleration is apparently due to the fact that vanadium acts as an intermediate in the solid-state exchange of the oxygen atoms for halogens. This assumption is in good agreement with mechanism proposed in the literature.[47,48]

TABLE II. MgO conversion and duration of induction period (τ_{ind}) during VO$_x$·MgO interaction with CF$_2$Cl$_2$ in TEOM microanalyzer at 350 °C

V loading, wt. % V$_2$O$_5$	MgO conversion, %	τ_{ind} / min
0	42	15
1	94	12
10	100	2

Complete MgO conversion was observed when the vanadium loading in the sample was as high as 10 wt. % (normalized to V$_2$O$_5$, Table II). The induction period was just 2 min. So, the presence of vanadium in MgO in significant amounts leads to faster and deeper reaction with the bulk of nanocrystalline MgO.

Complete conversion of AP–MgO doped with vanadium was confirmed by XRD. After reaction, the sample was found to consist of a well-crystallized MgF$_2$ phase. No peaks attributable to MgO were observed. The average crystallite size increased from 6 nm in the initial MgO to 38 nm in the resulting MgF$_2$. Apparently, several MgO nanoparticles merged to form a larger MgF$_2$ particle.

Samples with 1 and 10 wt. % V in nanocrystalline MgO were also prepared by mixing ammonium vanadate and AP-MgO. No vanadium-containing phases were identified by XRD for the samples with 1 % V. V$_2$O$_5$ was observed in addition to the cubic MgO phase for the samples with 10 % V. The average crystallite size of the V$_2$O$_5$ phase was about 20 nm. No phases of magnesium vanadates

were observed by XRD. Still, small vanadate clusters not observable by XRD might be formed on the MgO surface.

The effect of vanadium addition from ammonium vanadate on the AP-MgO reaction with CF_2Cl_2 is shown in Fig. 4. MgF_2 appears to be the only solid reaction product identifiable by XRD. Some MgO nanoparticles were not involved in the reaction with the halocarbon. The weight increase of 34 % observed in the experiment shown in Fig. 4 corresponds to the MgO conversion about 62 %. The fraction of the MgO nanoparticles involved in the reaction appears to depend on the reaction conditions, choice of the MgO sample, reactor and temperature.
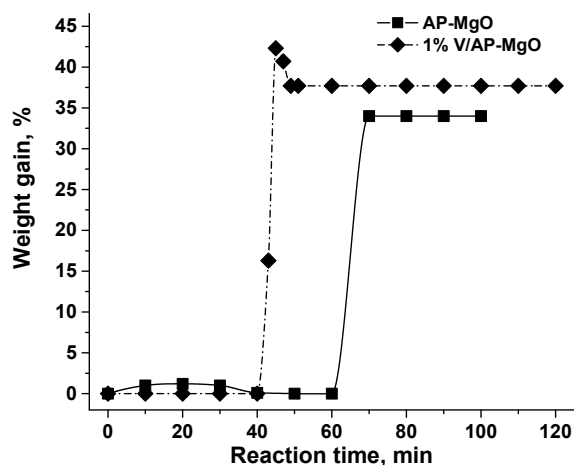

Fig. 4. Effect of vanadium concentration on reaction between AP––MgO and CF_2Cl_2 at 400 °C.

The introduction of 1 % V significantly shortened the induction period (Fig. 4). The MgO conversion grew to 69 %. Such result is similar to the one obtained for VO_x–MgO aerogel samples synthesized by co-gelation. The obtained results show that all stages of the reaction between nanocrystalline MgO and CF_2Cl_2 are significantly accelerated after vanadium addition. Vanadium species seems to act as a catalyst of the solid-state reaction reacting with the halocarbon faster than MgO.

Characterization of electron-donor and electron-acceptor sites during AP–MgO reaction with CF_2Cl_2

High activity of nanocrystalline MgO aerogels was usually attributed to high concentration of low-coordinated ions.[1] However, the obtained data for the reaction with CF_2Cl_2 clearly show that the active form of the destructive sorbent is formed only after induction period. Apparently, very active sites that do not exist before reaction are formed on the MgO surface during the induction period. The bulk solid-state reaction begins only when sufficient concentration of such sites is achieved.

The data reported above suggest that some intermediates, which are formed on the surface of vanadium-containing species, can then react with MgO. This reaction leads to faster formation of the active sites, which initiate the solid-state reaction between AP–MgO and CF_2Cl_2. Vanadia is a transition metal oxide widely used in selective catalytic oxidation.[5,10,49–51] Surface vanadyl groups are usually considered to be the active species of supported vanadia catalysts. Recent publications suggest that oxygen radicals may be present on the surface of supported vanadia catalysts and account for their activity in catalytic oxidation reactions.[52,53]

Different types of active sites have been identified on the MgO surface. These are conventional basic sites and low-coordinated surface ions, as well as highly active oxygen radical anions, electron-donor sites and acid sites identified using adsorption of nitroxyl radicals.[16,17,19,20] Oxygen radicals were observed on the MgO surface only after illumination in a vacuum installation and were not detected during reactions with halocarbons. Therefore, our main attention was attracted to highly active electron-donor and electron-acceptor sites. Earlier direct correlations were observed between the concentrations of such sites and the catalytic activity in low-temperature CO oxidation, n-butane isomerization and ethanol dehydration.[32,54,55]

A strong signal of TNB radical anions characterized by anisotropic splitting on a nitrogen atom with $A_{zz} = 27.2$ G was observed on the AP–MgO sample after activation in nitrogen flow without any reaction.[56] Its intensity on activated AP–MgO before reaction was about $6×10^{18}$ g^{-1}. The concentration of electron-donor sites gradually decreased during reaction with CF_2Cl_2 (Fig. 5). It took about 15 min for the signal to disappear. No correlation between the induction period length and the concentration of the electron-donor sites was observed. Although such sites may be involved in the surface reaction during the induction period, it is unlikely that they account for the bulk reaction between nano-crystalline MgO and CF_2Cl_2.
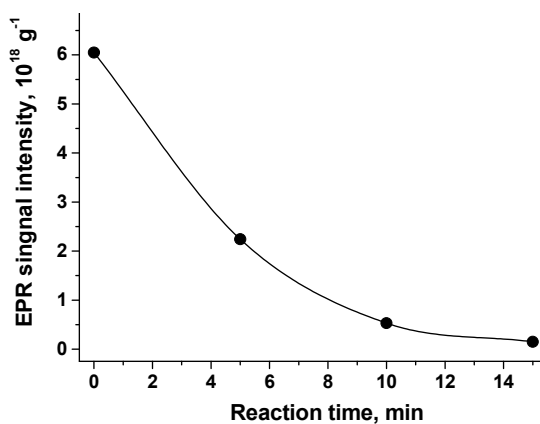

Fig. 5. Dependence of the EPR spectrum intensities observed after trinitrobenzene adsorption from toluene on AP-MgO on time of reaction with CF_2Cl_2.

On the contrary, the concentration of weak electron-acceptor sites tested using anthracene or perylene as the spin probes was found to correlate with the activity in the solid-state reaction. The ionization potentials of these compounds are 7.4 and 7.0 eV, respectively. Adsorption of these probes on AP–MgO after activation in nitrogen did not reveal the presence of any electron-acceptor sites. Heat treatment at 80 °C, which was reported to reveal weaker acceptor sites, led to the appearance of a singlet at $g = 2.003$ on the samples subjected to reaction with CF_2Cl_2 for different periods of time.[26,55] This signal can be attributed to polyaromatic structures formed by polycondensation of aromatic donor molecules on weak electron-acceptor sites.[22,26,55]

The intensities of the EPR signal at $g \approx 2.003$ observed after perylene adsorption on MgO and 5 % V–MgO aerogels after reaction with CF_2Cl_2 for different periods of time and after heating at 80 °C for 20 h are presented in Fig. 6. Almost no EPR signals resulting from the interaction with the spin probes were observed over AP–MgO until the reaction time of 10 min. At reaction times longer than 15 min the signal practically disappeared again. This means that electron-acceptor sites capable of ionizing perylene were present only on the AP–MgO sample subjected to reaction with CF_2Cl_2 for some time, most likely corresponding to the duration of the induction period. Independent measurements of the sample mass proved that this time approximately corresponds to the time when the solid-state reaction took place. Visible changes occurring with the sample volume corresponding to the bulk chemical reaction were also observed at the same moment.
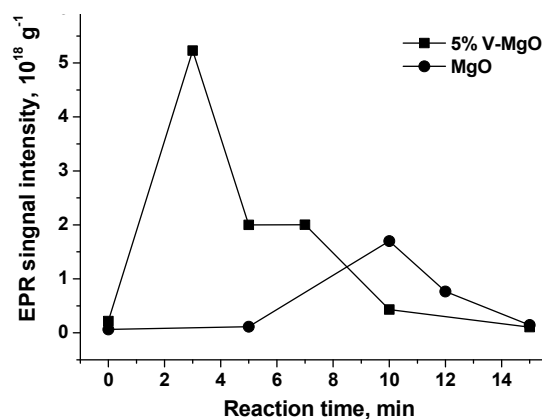

Fig. 6. Dependence of the EPR spectrum intensities observed after perylene adsorption from toluene on AP-MgO and 5%V_2O_5/AP-MgO on time of their reaction with CF_2Cl_2.

The induction period before the increase of the electron-acceptor sites concentration was much shorter on the sample with 5 % of vanadium than that on pure AP–MgO (Fig. 6). This result is in a good agreement with the kinetic data reported earlier.[13] Moreover, the concentration of electron-acceptor sites on this sample is higher. Overall, the results obtained in this study clearly prove that

there is a good correlation between the formation of weak electron-acceptor sites and the activity of nanocrystalline AP–MgO and AP–VO$_x$–MgO aerogels in the reaction with CF$_2$Cl$_2$.

The reported results demonstrate that weak electron-acceptor sites are accumulated on the MgO surface during the induction period of reaction with CF$_2$Cl$_2$. Apparently such sites are related to fluorine and/or chlorine atoms that are accumulated on the MgO surface during the induction period. Alumina modification with chlorine also increased the concentration of weak electron-acceptor sites tested using anthracene adsorption followed by heating at 80 °C.[55] They seem to be the most likely active sites for the fast solid-state reaction between nanocrystalline MgO and CF$_2$Cl$_2$.

Unfortunately, the structure of such sites is not known even for materials where they were extensively studied. According to the most common theories, the electron-acceptor sites could be Lewis acid sites accepting a single electron rather than an electron pair, Bronsted acid sites, or O$^-$ radicals.[22,55,57,58] Note that the electron-acceptor properties of conventional surface acid sites are not even close to the values required for ionization of the used aromatic probes. We think that only positively charged surface species can have the required electron affinity about 7 eV.

Simplified models of the electron-acceptor sites suggested by us are presented in Fig. 7. We believe that the electron-acceptor sites on the modified MgO surface are acid sites originating from separation of the charged fragments resulting in the surface polarization. These could be Lewis acid sites resulting from uncompensated oxygen substitution for chlorine and/or fluorine ions (Fig. 7A) or Bronsted acid sites formed by HCl/HF chemisorption (Fig. 7B). More experimental and theoretical studies are required to understand the properties of electron-acceptor sites on the surface of halogenated MgO and the mechanism of their involvement in the reaction with CF$_2$Cl$_2$.
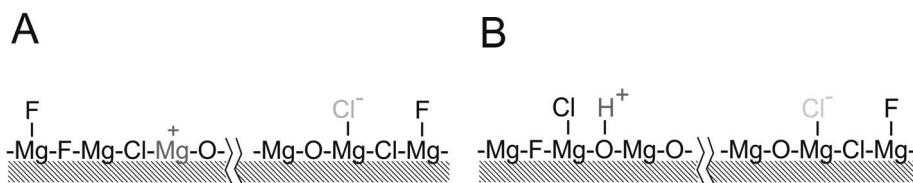

Fig. 7. Suggested structures of electron-acceptor sites on the surface of partially halogenated MgO.

CONCLUSION

Destructive sorption of CF$_2$Cl$_2$ on MgO aerogels is characterized by a long induction period after which fast solid-state reaction takes place. Apparently, active sites are accumulated on the surface during the induction period. Vanadia

addition to nanocrystalline MgO was found to shorten the induction period in the reaction with CF_2Cl_2. A method for characterization of electron-acceptor sites during solid-state and catalytic reactions was developed. Using this method we found a good correlation between the rate of the halocarbon destruction on AP-MgO and V_2O_5/AP–MgO and the concentration of weak electron-acceptor sites tested using perylene as a spin probe.

The studied electron-acceptor sites are definitely very active structures. Their high electron affinity about 7 eV implies that they are characterized by very high acidity. So, it is very important to study possible correlations between the concentrations of electron-acceptor sites and their activity in various catalytic and solid-state reactions. The technique developed by us can be used to study the concentrations of electron-acceptor sites of different strengths ex-situ at different reactions stages.

И З В О Д
ИСПИТИВАЊЕ ТРАНСФОРМАЦИЈЕ MgO У MgF_2 У ПРИСУСТВУ CF_2Cl_2

ALEKSEY A. VEDYAGIN[1,2], ALEXANDER F. BEDILO[1,3], ILYA V. MISHAKOV[1,2]
и EKATERINA I. SHUVARAKOVA[1,3]

[1]*Boreskov Institute of Catalysis, Siberian Branch, Russian Academy of Sciences, Novosibirsk, Russia,*
[2]*National Research Tomsk Polytechnic University, Tomsk, Russia and* [3]*Novosibirsk Institute of Technology, Moscow State University of Design and Technology, Novosibirsk, Russia*

Аерогелови оксида земноалкалих метала добијени сол–гел методом праћеном сушењем у аутоклаву су нанокристални мезопорозни материјали велике реактивности. Реакција у чврстом стању MgO аерогелова и CF_2Cl_2 се дешава након дугог индукционог периода, у току којег се активни центри акумулирају на површини наночестица. Нађено је да додатак ванадијума има ефекат промотера ове реакције убрзавајући процес формирања активних центара. Развијена је метода карактеризације електрон-акцепторских центара применом електрон-спинске резонантне спектроскопије коришћењем перилена као спинске пробе. Уочена је добра корелација између брзине деструктивне сорпције CF_2Cl_2 и концентрације слабих електрон-акцепторских центара. Дат је поједностављен модел таквих центара. Кисели центри на модификованој MgO површини потичу од наелектрисаних фрагмената и доводе до површинске поларизације. Некомпензована супституција кисеоника хлоридним и/или флуоридним јонима доводи до појаве Луис-ових киселих центара, док HCl/HF хемисорпција резултује у формирању Бронштедових центара.

REFERENCES

1. K. J. Klabunde, J. Stark, O. Koper, C. Mohs, D. G. Park, S. Decker, Y. Jiang, I. Lagadic, D. J. Zhang, *J. Phys. Chem.* **100** (1996) 12142
2. O. B. Koper, I. Lagadic, A. Volodin, K. J. Klabunde, *Chem. Mater.* **9** (1997) 2468

3. I. V. Mishakov, V. I. Zaikovskii, D. S. Heroux, A. F. Bedilo, V. V. Chesnokov, A. M. Volodin, I. N. Martyanov, S. V. Filimonova, V. N. Parmon, K. J. Klabunde, *J. Phys. Chem., B* **109** (2005) 6982
4. R. Richards, W. F. Li, S. Decker, C. Davidson, O. Koper, V. Zaikovski, A. Volodin, T. Rieker, K. J. Klabunde, *J. Am. Chem. Soc.* **122** (2000) 4921
5. V. V. Chesnokov, A. F. Bedilo, D. S. Heroux, I. V. Mishakov, K. J. Klabunde, *J. Catal.* **218** (2003) 438
6. B. M. Choudary, R. S. Mulukutla, K. J. Klabunde, *J. Am. Chem. Soc.* **125** (2003) 2020
7. P. P. Gupta, K. L. Hohn, L. E. Erickson, K. J. Klabunde, A. F. Bedilo, *AIChE J.* **50** (2004) 3195
8. I. V. Mishakov, A. F. Bedilo, R. M. Richards, V. V. Chesnokov, A. M. Volodin, V. I. Zaikovskii, R. A. Buyanov, K. J. Klabunde, *J. Catal.* **206** (2002) 40
9. I. V. Mishakov, D. S. Heroux, V. V. Chesnokov, S. G. Koscheev, M. S. Mel'gunov, A. F. Bedilo, R. A. Buyanov, K. J. Klabunde, *J. Catal.* **229** (2005) 344
10. I. V. Mishakov, A. A. Vedyagin, A. F. Bedilo, V. I. Zailovskii, K. J. Klabunde, *Catal. Today* **144** (2009) 278
11. Y. Jiang, S. Decker, C. Mohs, K. J. Klabunde, *J. Catal.* **180** (1998) 24
12. I. N. Martyanov, K. J. Klabunde, *J. Catal.* **224** (2004) 340
13. E. V. Ilyina, I. V. Mishakov, A. A. Vedyagin, A. F. Bedilo, K. J. Klabunde, *Microporous Mesoporous Mater.* **175** (2013) 76
14. A. F. Bedilo, A. M. Volodin, I. V. Mishakov, V. V. Chesnokov, E. V. Il'ina, I. V. Tokareva, E. I. Shuvarakova, *Kinet. Catal.* **55** (2014) 520
15. M. Chiesa, M. C. Paganini, G. Spoto, E. Giamello, C. Di Valentin, A. Del Vitto, G. Pacchioni, *J. Phys. Chem., B* **109** (2005) 7314
16. D. S. Heroux, A. M. Volodin, V. I. Zaikovski, V. V. Chesnokov, A. F. Bedilo, K. J. Klabunde, *J. Phys. Chem., B* **108** (2004) 3140
17. S. E. Malykhin, A. M. Volodin, A. F. Bedilo, G. M. Zhidomirov, *J. Phys. Chem., C* **113** (2009) 10350
18. I. D. P. R. Moreira, J. C. Wojdel, F. Illas, M. Chiesa, E. Giamello, *Chem. Phys. Lett.* **462** (2008) 78
19. R. M. Richards, A. M. Volodin, A. F. Bedilo, K. J. Klabunde, *Phys. Chem. Chem. Phys.* **5** (2003) 4299
20. A. M. Volodin, *Catal. Today* **58** (2000) 103
21. A. M. Volodin, S. E. Malykhin, G. M. Zhidomirov, *Kinet. Catal.* **52** (2011) 605
22. A. F. Bedilo, A. M. Volodin, *Kinet. Catal.* **50** (2009) 314
23. B. D. Flockhart, I. R. Leith, R. C. Pink, *J. Catal.* **9** (1967) 45
24. H. Garcia, H. D. Roth, *Chem. Rev.* **102** (2002) 3947
25. D. A. Medvedev, A. A. Rybinskaya, R. M. Kenzhin, A. M. Volodin, A. F. Bedilo, *Phys. Chem. Chem. Phys.* **14** (2012) 2587
26. A. F. Bedilo, E. I. Shuvarakova, A. A. Rybinskaya, D. A. Medvedev, *J. Phys. Chem., C* **118** (2014) 15779
27. B. D. Flockhart, I. R. Leith, R. C. Pink, *Trans. Faraday Soc.* **66** (1970) 469
28. T. A. Konovalova, A. F. Bedilo, A. M. Volodin, *React. Kinet. Catal. Lett.* **51** (1993) 81
29. A. F. Bedilo, A. M. Volodin, G. A. Zenkovets, G. V. Timoshok, *React. Kinet. Catal. Lett.* **55** (1995) 183
30. A. F. Bedilo, A. M. Volodin, *React. Kinet. Catal. Lett.* **67** (1999) 197
31. A. F. Bedilo, V. I. Kim, A. M. Volodin, *J. Catal.* **176** (1998) 294

32. A. F. Bedilo, A. S. Ivanova, N. A. Pakhomov, A. M. Volodin, *J. Mol. Catal., A: Chem.* **158** (2000) 409
33. A. F. Bedilo, A. V. Timoshok, A. M. Volodin, *Catal. Lett.* **68** (2000) 209
34. A. V. Timoshok, A. F. Bedilo, A. M. Volodin, *React. Kinet. Catal. Lett.* **59** (1996) 165
35. C. Sanchez, M. In, *J. Non-Cryst. Solids* **147** (1992) 1
36. U. Schubert, N. Husing, A. Lorenz, *Chem. Mater.* **7** (1995) 2010
37. A. F. Bedilo, K. J. Klabunde, *Nanostruct. Mater.* **8** (1997) 119
38. A. F. Bedilo, K. J. Klabunde, *J. Catal.* **176** (1998) 448
39. L. K. Campbell, B. K. Na, E. I. Ko, *Chem. Mater.* **4** (1992) 1329
40. Y. L. Diao, W. P. Walawender, C. M. Sorensen, K. J. Klabunde, T. Ricke, *Chem. Mater.* **14** (2002) 362
41. A. F. Bedilo, M. J. Sigel, O. B. Koper, M. S. Melgunov, K. J. Klabunde, *J. Mater. Chem.* **12** (2002) 3599
42. M. S. Mel'gunov, V. B. Fenelonov, E. A. Mel'gunova, A. F. Bedilo, K. J. Klabunde, *J. Phys. Chem., B* **107** (2003) 2427
43. S. Utamapanya, K. J. Klabunde, J. R. Schlup, *Chem. Mater.* **3** (1991) 175
44. P. N. Kapoor, D. Heroux, R. S. Mulukutla, V. Zaikovskii, K. J. Klabunde, *J. Mater. Chem.* **13** (2003) 410
45. J. B. Miller, E. I. Ko, *Catal. Today* **35** (1997) 269
46. R. Vidal-Michel, K. L. Hohn, *J. Catal.* **221** (2004) 127
47. T. Tamai, K. Inazu, K. Aika, *Chem. Lett.* **5** (2003) 436
48. T. Tamai, K. Inazu, K. Aika, *Bull. Chem. Soc. Jpn.* **78** (2005) 1565
49. B. Beck, M. Harth, N. G. Hamilton, C. Carrero, J. J. Uhlrich, A. Trunschke, S. Shaikhutdinov, H. Schubert, H. J. Freund, R. Schlogl, J. Sauer, R. Schomacker, *J. Catal.* **296** (2012) 120
50. I. V. Mishakov, E. V. Ilyina, A. F. Bedilo, A. A. Vedyagin, *React. Kinet. Catal. Lett.* **97** (2009) 355
51. I. E. Wachs, B. M. Weckhuysen, *Appl. Catal., A* **157** (1997) 67
52. V. I. Avdeev, A. F. Bedilo, *J. Phys. Chem., C* **117** (2013) 14701
53. V. I. Avdeev, A. F. Bedilo, *Res. Chem. Intermed.* **42** (2016) 5237
54. A. A. Vedyagin, A. M. Volodin, V. O. Stoyanovskii, I. V. Mishakov, D. A. Medvedev, A. S. Noskov, *Appl. Catal., B* **103** (2011) 397
55. R. A. Zotov, V. V. Molchanov, A. M. Volodin, A. F. Bedilo, *J. Catal.* **278** (2011) 71
56. A. F. Bedilo, E. I. Shuvarakova, A. M. Volodin, E. V. Ilyina, I. V. Mishakov, A. A. Vedyagin, V. V. Chesnokov, D. S. Heroux, K. J. Klabunde, *J. Phys. Chem., C* **118** (2014) 13715
57. D. N. Stamires, J. Turkevich, *J. Am. Chem. Soc.* **86** (1964) 749
58. M. J. Nash, A. M. Shough, D. W. Fickel, D. J. Doren, R. F. Lobo, *J. Am. Chem. Soc.* **130** (2008) 2460.